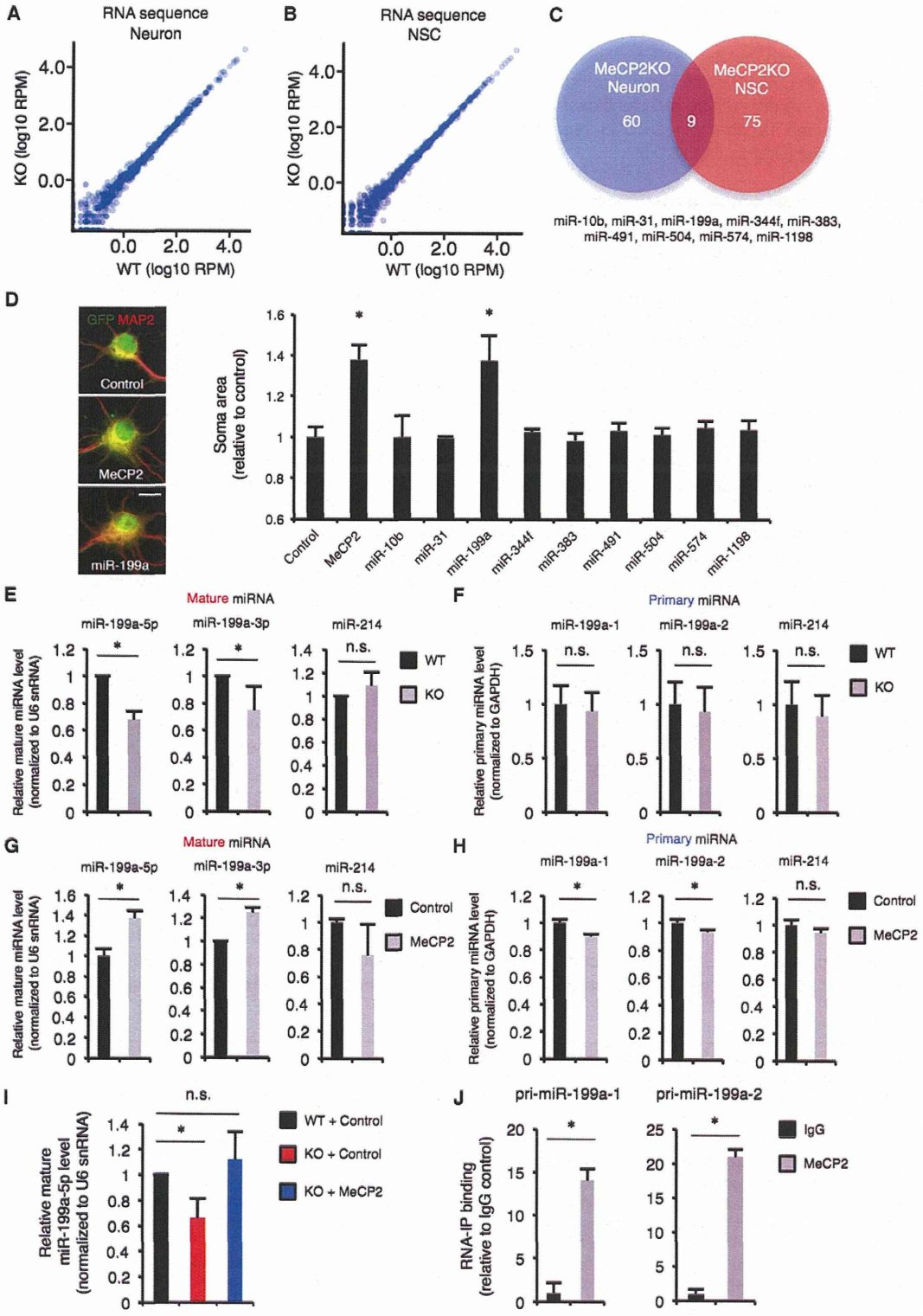

(legend on next page)

the core components of the Drosha complex, both in vitro and in vivo.

Recent work has reported that MeCP2 interferes with the association of Drosha with DGCR8 in the Drosha complex (Cheng et al., 2014). However, we did not find any significant change in the association between Drosha and DGCR8 regardless of MeCP2 expression level (Figures S1E–S1H).

MeCP2 Regulates Processing of a Specific miRNA

To identify target miRNAs of the MeCP2-Drosha complex, we performed deep RNA sequencing using a small non-coding RNA fraction extracted from neurons and NSCs of wild-type (WT) and KO mice. No drastic and/or overall alterations of mature miRNA expression levels were observed in either cell type (Figures 2A and 2B), suggesting that MeCP2 does not affect core Drosha-DGCR8 microprocessor function. We then searched for miRNAs whose level decreased over 1.5-fold in MeCP2-KO cells compared with WT. Sixty and 75 miRNAs were reduced in MeCP2-KO neurons and NSCs, respectively (Figure 2C). Since MeCP2 associates with the Drosha complex in both cell types, we focused on miRNAs that decreased in both cell types and found nine that met this criterion.

We then performed functional screening for mTOR signal-regulating miRNAs that act downstream of MeCP2. We expressed the nine miRNAs in hippocampal neurons and evaluated neuronal soma size, since mTOR signaling is known to regulate cellular soma size, and found that only miR-199a increased the neuronal soma size to a similar extent as MeCP2 expression did (Figure 2D). We also found that miR-199a expression and blockade (see below for details) potentiated and attenuated, respectively, the phosphorylation levels in neurons of S6 ribosomal protein, which signify the activation of mTOR signaling, indicating that miR-199a positively regulates mTOR signaling activity (Figures S2A and S2B). Therefore, we decided to focus on miR-199a in the following experiments.

miR-199a is expressed from two genomic loci, *miR-199a-1* and *miR-199a-2*, and pri-miR-199a-2 is synthesized with pri-miR-214 as a single transcript (Lee et al., 2009). Two types of mature form, miR-199a-5p and -3p, are generated from both *miR-199a-1* and *miR-199a-2* (Figure S2C), but no function of miR-199a in the nervous system has yet been reported. To determine whether MeCP2 specifically regulates posttranscriptional processing of miR-199a, we first measured the expression levels of primary and mature forms of miR-199a and miR-214, by qRT-PCR, in hippocampal neurons from WT and MeCP2-KO mice. We found that the mature forms miR-199a-5p and miR-199a-3p were downregulated in MeCP2-KO neurons (Figure 2E); the same held true in MeCP2-KO NSCs (Figure S2D), as reported previously (Szulwach et al., 2010). In contrast, pri-miR-199a-1 and -2 levels showed no significant change in MeCP2-KO neurons compared with those in WT neurons (Figure 2F), suggesting that the reduced mature-form levels were not caused by decreased levels of transcription. In addition, expression levels of the mature forms of miR-214 and miR-137, the latter previously identified as a transcriptional repression target of MeCP2 in NSCs (Szulwach et al., 2010), were unchanged (Figures 2E and 2F; Figures S2D and S2E). Conversely, overexpression of MeCP2 in WT neurons led to significant increases of mature miR-199a-5p and -3p but not of mature miR-214 (Figure 2G). Expression of primary miR-199a and miR-214 was either unchanged or slightly reduced in response to MeCP2 overexpression in WT neurons (Figure 2H). To further determine whether MeCP2 regulates the expression of miR-199a, we also re-expressed MeCP2 in MeCP2-KO neurons. As expected, this restored the level of mature-miR-199a expression to that in WT neurons (Figure 2I). No change in the mature miR-137 expression level was observed (Figure S2E). Together, these results suggest that MeCP2 modulates specifically the posttranscriptional processing of pri-miR-199a, rather than its transcription. Dysregulation of miR-199a expression at posttranscriptional level was also observed in the frontal cortex of RTT patients (Table S1; Figures S2F and S2G), suggesting that the reduction of miR-199a expression may associate with RTT pathophysiology.

We then examined the in vivo association of pri-miR-199a with the MeCP2 complex by RNA immunoprecipitation assay and found that both pri-miR-199a-1 and pri-miR-199a-2 clearly associated with the complex (Figure 2J). We also performed an in vitro pri-miRNA processing assay by incubating radiolabeled pri-miR-199a-2 substrate with anti-FLAG antibody immunoprecipitates from Neuro2A cells transfected with empty vector (mock), or with FLAG-tagged MeCP2- or FLAG-tagged Drosha-expressing constructs. pri-miR-199a-2 processing activity in the MeCP2 complex immunoprecipitates was comparable to that in Drosha complex immunoprecipitates, and higher than

Figure 2. MeCP2 Regulates Posttranscriptional Processing of a Specific miRNA

(A and B) Scatterplot of miRNA expression levels ($\log_{10}$) in neurons (A) or NSCs (B) from WT and MeCP2-KO, respectively.

(C) Venn diagram showing the overlap of miRNAs whose levels are lower in MeCP2-KO neurons and NSCs than in WT. Nine miRNAs, listed below the diagram, overlap in the two cell types.

(D) Functional screening for mTOR signaling-related miRNA that acts downstream of MeCP2. The nine miRNAs identified in (C) were expressed in WT hippocampal neurons and neuronal soma size was evaluated. (*$p < 0.05$ compared to control; $n = 3$). Representative images of neurons stained with anti-MAP2 (red) and -GFP (green) antibodies. P0 WT hippocampus-derived neurons were infected with lentiviruses expressing GFP alone (control) or GFP together with MeCP2 or primary-miR-199a and cultured for 10 days. Scale bar, 10 μm (left). Quantitative analysis of the functional screening (right).

(E and F) Expression levels of mature (E) and primary (F) forms of the indicated miRNAs were examined in WT and MeCP2-KO hippocampal neurons by qRT-PCR analysis (*$p < 0.05$ compared to WT; n.s., not significantly different; $n = 3$).

(G and H) Expression levels of mature (G) and primary (H) forms of the indicated miRNAs were examined in hippocampal neurons infected with control and MeCP2-expressing lentiviruses by qRT-PCR analysis (*$p < 0.05$ compared to control; n.s., not significantly different; $n = 3$).

(I) Exogenous MeCP2 expressed by a recombinant lentivirus could restore the miR-199a-5p expression levels in MeCP2-KO hippocampal neurons to those seen in WT hippocampal neurons (*$p < 0.05$ compared to WT; n.s., not significantly different; $n = 3$).

(J) RIP analysis of the association of pri-miR-199a-1 and pri-miR-199a-2 with MeCP2 in P1 hippocampal neurons. Immunoprecipitation was performed using control IgG and anti-MeCP2 antibody (*$p < 0.05$ compared to IgG; $n = 3$).

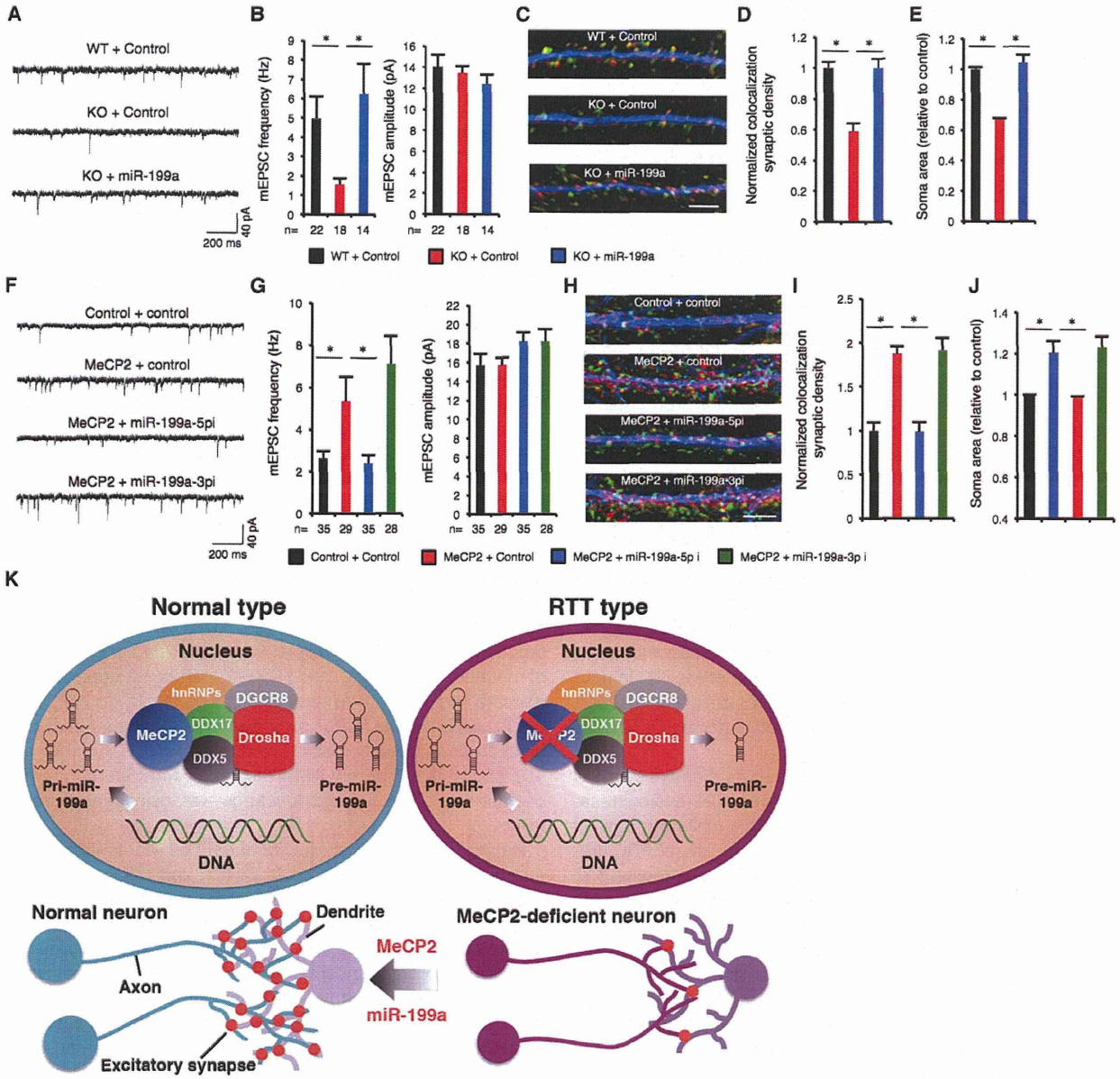

Figure 3. miR-199a Overcomes Neuronal Abnormalities Caused by the Loss of MeCP2 and Acts Downstream of MeCP2

(A) Representative traces of individual mEPSC frequency recordings. P0–P2 WT and MeCP2-KO hippocampal neurons were infected with lentiviruses expressing GFP alone (control) or GFP together with the precursor form of miR-199a and cultured for 10–14 days.

(B) Quantification of mEPSC frequency and amplitude in (A). The number of neurons analyzed is shown under each bar.

(C) Representative images of cultured hippocampal neurons as indicated, stained with antibodies against VGLUT1 (green), PSD-95 (red), and MAP2 (blue). Scale bar, 5 μm.

(D) Normalized densities of colocalized VGLUT1 and PSD-95 signal in the hippocampal cultures in (C) were quantified (n = 10 neurons per group).

(E) Quantification of neuronal soma size relative to control WT neurons. n = 3 independent experiments; in each experiment at least 100 neurons were assessed.

(F) Representative traces of individual mEPSC frequency recordings of WT hippocampal neurons co-infected with control or MeCP2-expressing lentiviruses and those expressing sponge miRNA inhibitors against either miR-199a-5p or miR-199a-3p.

(G) Quantification of mEPSC frequency and amplitude in (F). The number of neurons analyzed is shown under the bars.

(H) Representative images of cultured hippocampal neurons as indicated, stained with antibodies against VGLUT1 (green), PSD-95 (red), and MAP2 (blue). Scale bar, 5 μm.

(legend continued on next page)

that in immunoprecipitates from mock-transfected cells (Figures S2H and S2I). Moreover, Drosha complex from MeCP2-knockdown cells showed lower processing activity against pri-miR-199a than that from control cells (Figures S2J and S2K). In contrast, processing activity by the Drosha immunoprecipitates against pri-miR-214 was similar regardless of MeCP2 expression levels. Taken together, these results indicate that MeCP2 specifically contributes to the posttranscriptional processing of pri-miR-199a.

miR-199a Acts Downstream of MeCP2 In Vitro and In Vivo

MeCP2 target molecules that can rescue major RTT neuronal phenotypes such as decreased excitatory synaptic transmission, synaptic density, and soma size have not been identified. Therefore, we investigated whether miR-199a, identified here as a MeCP2 target, restores RTT neuronal properties of MeCP2-deficient neurons.

MeCP2-KO neurons displayed a significantly lower miniature excitatory postsynaptic current (mEPSC) frequency, lower synaptic density, and smaller soma size than WT neurons, as reported previously (Chao et al., 2007; Nelson et al., 2006) (Figures 3A–3E). These impairments were overcome by the re-introduction of MeCP2 (Figures S3A–S3E). Likewise, expression of precursor form miR-199a in MeCP2-KO neurons completely restored RTT neuronal phenotypes such as decreased mEPSC frequency, excitatory synaptic density, and soma size, indicating that miR-199a can substitute for the function of MeCP2 in neurons (Figures 3A–3E; Figures S3F and S3G). No significant differences in mEPSC amplitude were observed under any conditions (Figures 3A–3E).

To determine whether miR-199a indeed acts downstream of MeCP2, we inhibited miR-199a function in MeCP2-overexpressing WT hippocampal neurons using miRNA inhibitors against miR-199a-5p or miR-199a-3p. The increase of mEPSC frequency and synaptic density as well as the enlargement of neuronal soma size induced by MeCP2 overexpression were abolished when the cells were treated with miR-199a-5p inhibitor but not with control or miR-199a-3p inhibitor (Figures 3F–3J). Although miR-134 was reported to act downstream of MeCP2 (Cheng et al., 2014), the expression of miR-134 in neurons did not influence the effects of MeCP2 overexpression in our experimental setting (Figures S3H–S3L).

To test whether blocking endogenous activities of miR-199a recapitulates the RTT neuronal phenotype, we treated WT hippocampal neurons with miRNA inhibitors against miR-199a-5p or miR-199a-3p. In contrast to scrambled control and miR-199a-3p inhibitor, treatment with an inhibitor of miR-199a-5p resulted in a significant reduction of mEPSC frequency, synaptic density, and soma size (Figures S3M–S3Q). We also observed that overexpression of miR-199a in WT hippocampal neurons phenocopied MeCP2 overexpression (Figures S3R–S3V). We further demonstrated that inhibition of endogenous miR-214 and expression of miR-214 could not abolish the effect of MeCP2 expression (mEPSC) (Figures S3W and S3X) and could not restore the RTT neuronal phenotypes (synaptic density and soma size) (Figures S3Y and S3Z), respectively. When we performed in utero electroporation to mouse embryonic brains, the effects of MeCP2 and miR-199a on soma size observed in vitro could be reproduced in vivo (data not shown). These results strongly indicate that miR-199a, specifically miR-199a-5p, is a direct MeCP2 target that critically contributes to MeCP2 functions (Figure 3K).

miR-199a Targets Inhibitory Factors of the mTOR Signaling Pathway

To identify target genes downstream of miR-199a that are physiologically relevant to RTT pathogenesis, we searched for mTOR signal-inhibiting genes that have miR-199a-5p target sequences in their 3′ UTRs using public databases including TargetScan 5.1, miRDB, Pictor, and miRanda. This search yielded three candidate genes: *Pde4d*, *Sirt1*, and *Hif1α* (Ghosh et al., 2010; Kim et al., 2010; Wouters and Koritzinsky, 2008) (Figure 4A). To examine whether these genes are actual targets of miR-199a, we conducted luciferase assays using reporter constructs harboring 3′ UTR of each gene, within which were native or mutated sequence complementary to the miR-199a seed sequence, in hippocampal neurons. The luciferase activities of native *Pde4d*, *Sirt1*, and *Hif1α*-3′ UTR constructs were all reduced significantly by miR-199a expression, whereas those of mutated *Pde4d*, *Sirt1*, and *Hif1α*-3′ UTR constructs were unaffected (Figure 4B). We then examined protein levels of PDE4D, SIRT1, and HIF1α in MeCP2-KO brain and found that they were indeed upregulated compared to those in WT (Figures 4C and 4D), suggesting that miR-199a targets *Pde4d*, *Sirt1*, and *Hif1α* downstream of MeCP2 and downregulates their cognate protein levels.

Having suggested that MeCP2 and miR-199a are epistatic to and negatively regulate PDE4D, SIRT1, and HIF1α, we tested whether expression of these mTOR signal negative regulators reverses the effect of MeCP2 expression in neurons. Because HIF1α is degraded through hydroxylation of specific proline residues in a normal atmosphere, we used in this experiment a constitutively active form of HIF1α (HIF1α-CA) whose hydroxylation-targeted proline residues are substituted by alanine (Jaakkola et al., 2001). The expression of *Pde4d*, *Sirt1*, and *Hif1α* (without their cognate 3′ UTR) abolished the enhanced mEPSC frequency, the increase in synapse number, and the enlarged soma size induced by MeCP2 overexpression (Figures 4E–4S). Interestingly, *Pde4d*, *Sirt1*, and *Hif1α*-CA with their native 3′ UTR sequences failed to abolish these effects of MeCP2 overexpression, while constructs with a 3′ UTR harboring a mutation in the miR-199a-target sequence significantly attenuated the effects of MeCP2 (Figures 4E–4S), indicating that miR-199a plays a critical role in controlling the expression of these mTOR signal inhibitors.

(I) Normalized densities of colocalized VGLUT1 and PSD-95 signals in the hippocampal cultures in (H) were quantified (n = 10 neurons per group).
(J) Quantification of neuronal soma size relative to control WT neurons. n = 3 independent experiments; in each experiment at least 100 neurons were assessed.
(K) Models of the regulation of miRNA processing by the MeCP2-Drosha complex in normal and RTT cells, and of the resultant neuronal phenotypes. Data are represented as mean ± SEM. *p < 0.05.

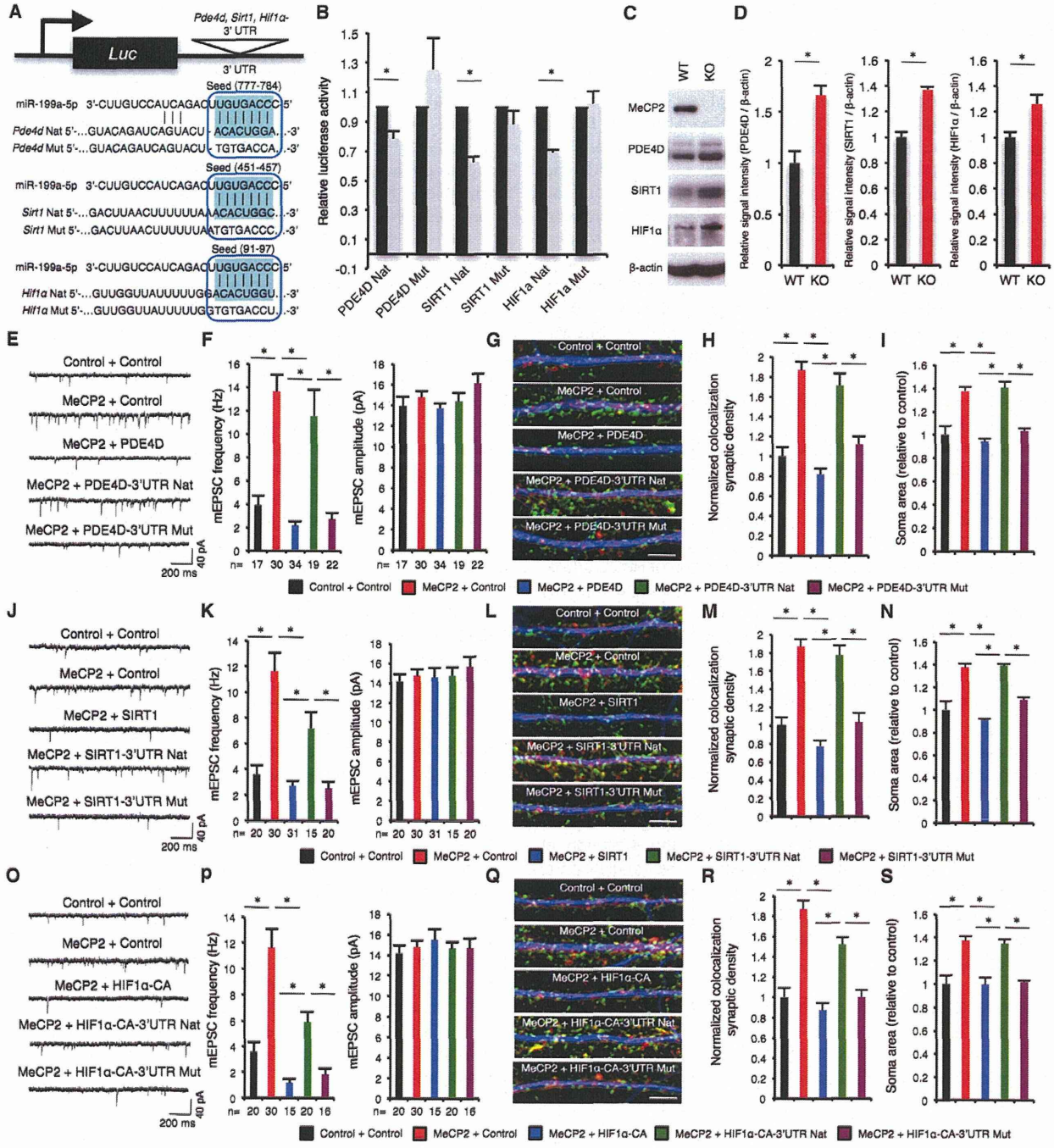

Figure 4. Three Negative Regulators of mTOR Signaling Are Functional Downstream Targets of miR-199a

(A and B) Luciferase reporter assays of the predicted miR-199a target genes. Schematics of luciferase assay reporter constructs are shown in (A). The miR-199a-5p seed sequence, miR-199a-5p target (upper, Nat), and its mutated (lower, Mut) sequences of each gene's 3′ UTR is indicated (blue boxes). The mir-199a-5p seed and its target sequences in *Pde4d*, *Sirt1*, and *Hif1α* 3′ UTRs are highlighted in light blue. Reduction of luciferase activity of *Pde4d*, *Sirt1*, and *Hif1α* 3′ UTRs with native miR-199a-5p sequences was observed (B). Data are represented as mean ± SEM. $^*p < 0.05$. n = 3 independent experiments.

(C) Western blot analysis showing that protein levels of PDE4D, SIRT1, and HIF1α are upregulated in MeCP2-KO brain (P1 cortex).

(D) Quantification of protein levels of PDE4D, SIRT1, and HIF1α. n = 3 brains from each genotype.

(E–S) PDE4D, SIRT1, and HIF1α act downstream of MeCP2/miR-199a.

(legend continued on next page)

We next asked whether the inhibition of these miR-199a downstream targets ameliorated RTT neuronal phenotypes. When we pharmacologically inhibited PDE4D with rolipram and SIRT1 with nicotinamide (NIC) and EX527, the defects in mEPSC, synaptic density, and soma size of MeCP2-KO neurons were all overcome (Figures S4A–S4O). Knockdown of *Pde4d* also remarkably restored these RTT neuronal phenotypes (Figures S4P–S4T). In addition, treatment with rolipram, NIC, and EX527 significantly recovered the neuronal impairments induced by the inhibition of miR-199a-5p (Figures S4U–S4D′). Moreover, when PDE4D, SIRT1, and HIF1α-CA were expressed in WT hippocampal neurons, similar neuronal impairments to those caused by MeCP2 deficiency and miR-199a inhibition were observed (Figures S4E′–S4J′). Taken together, these data support our model that *Pde4d*, *Sirt1*, and *Hif1α* are functional downstream targets of miR-199a in RTT neuropathology.

mTOR Underlies MeCP2-Related RTT Neuronal Phenotypes

Although the mTOR signaling pathway is dysregulated in MeCP2-deficient mice and cells (Li et al., 2013; Ricciardi et al., 2011), it has not been ascertained that mTOR signaling indeed functions downstream of MeCP2. Therefore, we first investigated whether activation of mTOR signaling ameliorates RTT neuronal phenotypes. We found that expression of Rheb, an upstream activator of mTOR, in MeCP2-KO hippocampal neurons clearly restored the neuronal impairments observed in MeCP2-KO neurons affecting mEPSC, synaptic density, and soma size (Figures 5A–5E). Moreover, activation of mTOR signaling by Rheb expression reversed the defects in neurons induced by miR-199a-5p inhibition and by PDE4D, SIRT1, and HIF1α-CA expression (Figures 5F–5J; Figures S5A–S5O). In support of these results, inhibition of mTOR by rapamycin strikingly abrogated the effects induced by MeCP2 and miR-199a expression, and by the pharmacological inhibition of miR-199a targets (PDE4D with rolipram and SIRT1 with EX527) (Figures 5K–5T; Figures S5P–S5Y). Furthermore, activation and inhibition of mTOR signaling in WT hippocampal neurons recapitulated the gain and loss of MeCP2 phenotypes, respectively (Figures S5Z–S5I′). Collectively, these findings demonstrate that mTOR signaling underlies MeCP2-related RTT phenotypes in neurons (Figures 5U and 5V).

Loss of *miR-199a-2* Recapitulates RTT Phenotypes In Vivo

miR-199a-1 KO mice had already been produced and do not display any gross physical or behavioral abnormalities (information from The Jackson Laboratory: http://jaxmice.jax.org/strain/017512.html) (Park et al., 2012), and it has been reported that the *Dnm3os* KO mice, which lack both *miR-199a-2* and *miR-214*, show similar skeletal abnormality and growth retardation to Rett patients and *MeCP2* KO mice (O'Connor et al., 2009; Watanabe et al., 2008). In contrast, *miR-214* single KO mice develop normally (Aurora et al., 2012), clearly indicating that the phenotypes observed in *Dnm3os* KO mice are attributable to the lack of *miR-199a-2*. Based on these observations, we further investigated the functions of miR-199a by establishing *miR-199a-2* KO mice using conventional method (Figures S6A–S6C). To our surprise, *miR-199a-2* KO mice displayed many RTT features that were similar to MeCP2 KO mice (Chen et al., 2001; Guy et al., 2001). We observed a marked reduction in size and body weight of the *miR-199a-2* KO mice compared to WT littermates, while *miR-199a-2*$^{-/+}$ heterozygotes are almost indistinguishable from WT (Figures 6A, 6B, and 6D). Brain size was also smaller in *miR-199a-2* KO mice (Figure 6C). Although most *miR-199a-2* KO mice appeared normal for the first ~3 postnatal weeks, but they then developed abnormal behavior, such as a stiff, uncoordinated gait, body trembling, pilar erection, irregular breathing, and hypoactivity (Figure 6E), and began to die at around 6 weeks (Guy et al., 2007). Immunohistochemical analysis revealed that *miR-199a-2* KO mice had normal brain architecture (Figures 6F and 6G), whereas their hippocampal and cortical neurons exhibited a smaller cell body and nucleus (Figures 6H–6K) regardless of MeCP2 expression (Figure S6D). In addition, we found that these neurons in *miR-199a-2* KO mice were more densely packed than those in WT, consistent with findings in RTT patients and MeCP2 KO mice (Figures 6H–6K) (Bauman et al., 1995; Chen et al., 2001; Guy et al., 2001). Taken together, these results indicate that miR-199a is a critical downstream target of MeCP2 for RTT phenotypes in vivo.

Loss of *miR-199a-2* Results in Decreased mTOR Activity in the Brain

To ask whether miR-199a regulates mTOR signaling in the brain, we assessed mTOR activity in the WT and *miR-199a-2* KO brain. Concordant with our hypothesis that miR-199a positively regulates mTOR activity, immunohistochemical analysis showed a striking reduction of pS6-positive neurons in the cortex and hippocampus of *miR-199a-2* KO mice (Figure 7). Collectively, these data suggest that miR-199a activates mTOR activity in vivo and that the MeCP2/miR-199a/mTOR axis makes a substantial contribution to RTT pathophysiology.

(E–I) Expression of PDE4D attenuates the effect of MeCP2 expression. Expression of PDE4D abrogates enhanced mEPSC frequency (E and F), increased number of excitatory synapses (G and H), and enlargement of soma area (I) in MeCP2-expressing neurons.

(J–N) Expression of SIRT1 abolishes the effect of MeCP2 expression. Expression of SIRT1 abrogates enhanced mEPSC frequency (J and K), increased number of excitatory synapses (L and M), and enlargement of soma area (N) in MeCP2-expressing neurons.

(O–S) Expression of HIF1α-CA attenuates the effect of MeCP2 expression. Expression of HIF1α-CA abrogates enhanced mEPSC frequency (O and P), increased number of excitatory synapses (Q and R), and enlargement of soma area (S) in MeCP2-expressing neurons. Note that the *Pde4d*, *Sirt1*, and *Hif1α* expression vector containing each native 3′ UTR (PDE4D-3′ UTR Nat, SIRT1-3′ UTR Nat, and HIF1α CA-3′ UTR Nat) was not effective in attenuating the effects of MeCP2. In contrast, the *Pde4d*, *Sirt1*, and *Hif1α* expression vector containing each mutated 3′ UTR (PDE4D-3′ UTR Mut, SIRT1-3′ UTR Mut, and HIF1α CA-3′ UTR Mut) efficiently abrogated the effects of MeCP2. Data are represented as mean ± SEM. *$p < 0.05$. The number of neurons analyzed is shown under the bars. Scale bars, 5 μm. Regarding quantification of neuronal soma size, n = 3 independent experiments; in each experiment, at least 100 neurons were assessed.

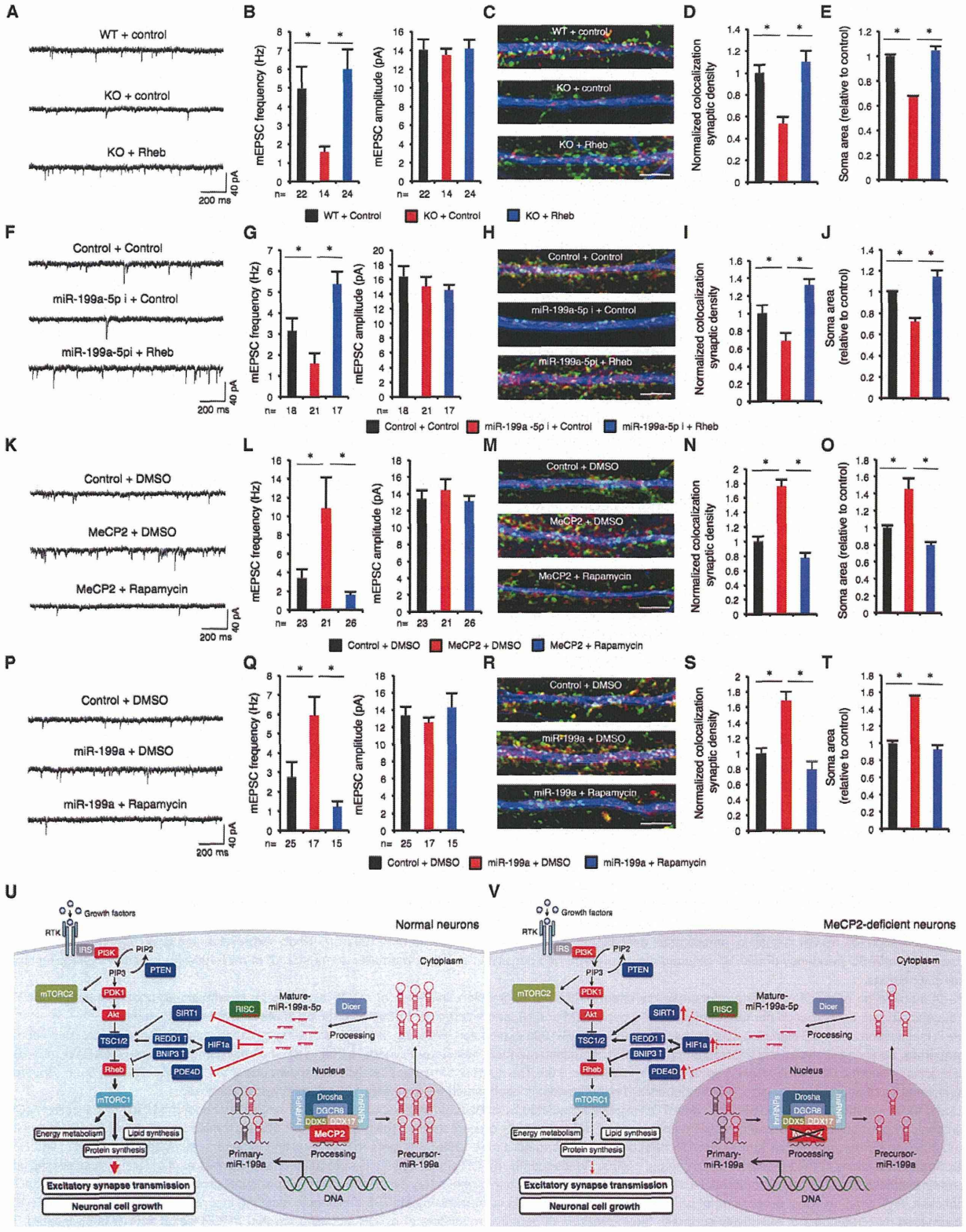

(legend on next page)

DISCUSSION

In this study, we demonstrated that MeCP2 facilitates specific miRNA processing as a component of Drosha complex and identified miR-199a as a direct MeCP2 target. We also revealed that exogenous miR-199a could overcome several impairments in MeCP2-KO neurons, and that inhibition of endogenous miR-199a abolished the effect of MeCP2 overexpression. Taken together, these results provide strong evidence that miR-199a is a direct MeCP2 target underlying the RTT phenotype. It has been reported recently that the interaction between Drosha and DGCR8 was attenuated in the brain lysate of MeCP2-overexpresing transgenic mice due to the competition of MeCP2 with Drosha for binding to DGCR8, suggesting MeCP2 has a negative role in miRNA processing. However, in our experimental setting using embryonic hippocampal neurons, overexpression of MeCP2 did not interfere with association of Drosha with DGCR8 and enhanced the specific miRNA processing (Figures S5C and S5D; Figure 2G). Although currently we do not have specific explanation of how MeCP2 exerts these opposite functions in miRNA processing, it could be, e.g., because of that posttranslational modification status of MeCP2 is different among different brain regions and neuronal subtypes, since phosphorylation of MeCP2 is known to alter MeCP2 functions (Tao et al., 2009). To verify the molecular mechanism is also an important challenge for future studies.

In the present study, we demonstrated that MeCP2 associates with pri-miR-199a-1 and pri-miR-199a-2. Nevertheless, how MeCP2 recognizes its target miRNAs remains elusive. Since pri-miR-199a-1 and pri-miR-199a-2 have exactly the same sequence in their mature miRNA regions but are completely different on the outsides, it is tempting to speculate that mature miRNA sequence is responsible for defining the specificity of MeCP2. In this relation, it has been indicated that transcription factor Smad1 directly binds to the cognate sequence within the mature sequence of target primary miRNA (Davis et al., 2010). However, precise consensus sequence of MeCP2 binding has not so far been determined, and we could not identify any common sequence among mature sequences in the miRNA suggested as MeCP2 targets in this study; we cannot rule out a possibility that other factors, such as conformation and methylation state of the outside regions, can play a critical role on regulating the MeCP2 binding specificity.

Although it has been assumed that a reduction of mTOR signal activity is involved in RTT pathogenesis, plausible molecular link between MeCP2 and the mTOR signaling pathway have been scant. Our findings clearly reveal a role for MeCP2 in the regulation of the mTOR signaling pathway as well as a previously unknown miRNA-based mechanism by which MeCP2 controls neuronal functions, which could clearly explain RTT pathophysiology (Figures 5U and 5V). Most importantly, we have demonstrated that genetic deletion of *miR-199a-2* attenuates mTOR activity in the brain and recapitulates numerous features of RTT patients and MeCP2 KO mice, supporting the idea that the MeCP2/miR-199a/mTOR axis is deeply involved in RTT phenotypes. Based on these findings, we propose that dysregulation of the MeCP2/miR-199a/mTOR axis contributes to the pathogenesis of neurodevelopmental disorders, and that an avenue for the development of an effective therapeutic strategy against RTT is to control molecules involved in this pathway.

EXPERIMENTAL PROCEDURES

See Supplemental Experimental Procedures for additional details.

RNA Immunoprecipitation

Co-immunoprecipitation of RNAs with anti-MeCP2 antibody and their subsequent isolation were performed using a RiboCluster Profiler RIP-Assay kit (MBL International Corporation) according to the manufacturer's protocol. Whole-cell lysates were sonicated and used for the RNA immunoprecipitation assay. Rabbit immunoglobulin G (IgG) supplied by the manufacturer was used as a control and the immunoprecipitated RNA was analyzed by qRT-PCR using a TaqMan pri-microRNA assay kit (Applied Biosystems) with specific primers.

Luciferase Assay

Hippocampal neurons were co-transfected with control (pLLX) or miR-199a expression vector and pmirGLO-*Pde4d*, *Sirt1*, *Hif1α*-3′ UTR-Nat or

Figure 5. mTOR Signaling Regulates Neuronal Phenotype Downstream of MeCP2

(A–E) Activation of mTOR signaling overcomes RTT neuronal phenotypes. Rheb expression rescues the decreased mEPSC frequency (A and B), reduced excitatory synaptic density (C and D), and smaller soma size (E) of MeCP2-KO hippocampal neurons.

(F–J) Activation of mTOR signaling ameliorates deficits caused by the inhibition of miR-199a-5p. Rheb expression restores abnormalities such as decreased mEPSC frequency (F and G), reduced excitatory synaptic density (H and I), and smaller soma size (J) of miR-199a-5p inhibitor-expressing hippocampal neurons.

(K–O) Inactivation of mTOR signaling attenuates the effect of MeCP2 expression. Inhibition of mTOR signaling by rapamycin abrogates enhanced mEPSC frequency (K and L), increased number of excitatory synapses (M and N), and enlargement of soma area (O) of MeCP2-expressing neurons.

(P–T) Inactivation of mTOR signaling attenuates the effects of miR-199a expression. Blocking of mTOR signaling by rapamycin abolished potentiated neuronal properties, such as enhanced mEPSC frequency (P and Q), increased number of excitatory synapses (R and S), and enlargement of soma area (T) of miR-199a-expressing neurons. Data are represented as mean ± SEM. *$p < 0.05$. The number of neurons analyzed is shown under the bars. Scale bars, 5 μm. Regarding quantification of neuronal soma size, n = 3 independent experiments; in each experiment, at least 100 neurons were assessed.

(U and V) Schematic link between MeCP2 and mTOR signaling mediated by miRNA biogenesis, explaining RTT neuronal phenotype U. In normal cells, MeCP2-Drosha complex facilitates processing of the primary form of miR-199a to its precursor form. The precursor miR-199a is translocated to the cytoplasm and then subjected to further processing to mature miR-199a by Dicer. The mature miR-199a-5p targets mTOR signaling inhibitors, such as *Pde4d*, *Sirt1*, and *Hif1α*, leading to reductions in the levels of their cognate proteins. Consequently, mTOR signal activity is upregulated, and downstream cellular processes including protein synthesis are eventually promoted. As a result, neuronal functions such as excitatory synaptic transmission and cell growth are potentiated. (V) In MeCP2-deficient (RTT type) neurons, processing of pri-miR-199a to pre-miR-199a is impaired by MeCP2 deficiency, resulting in a reduced level of mature miR-199a. Decreased miR-199a cannot effectively suppress the expression of negative regulators of mTOR signaling, so that mTOR signal activity is attenuated. This attenuation of mTOR signaling induces RTT neuronal phenotypes including diminished excitatory synaptic transmission and cell growth.

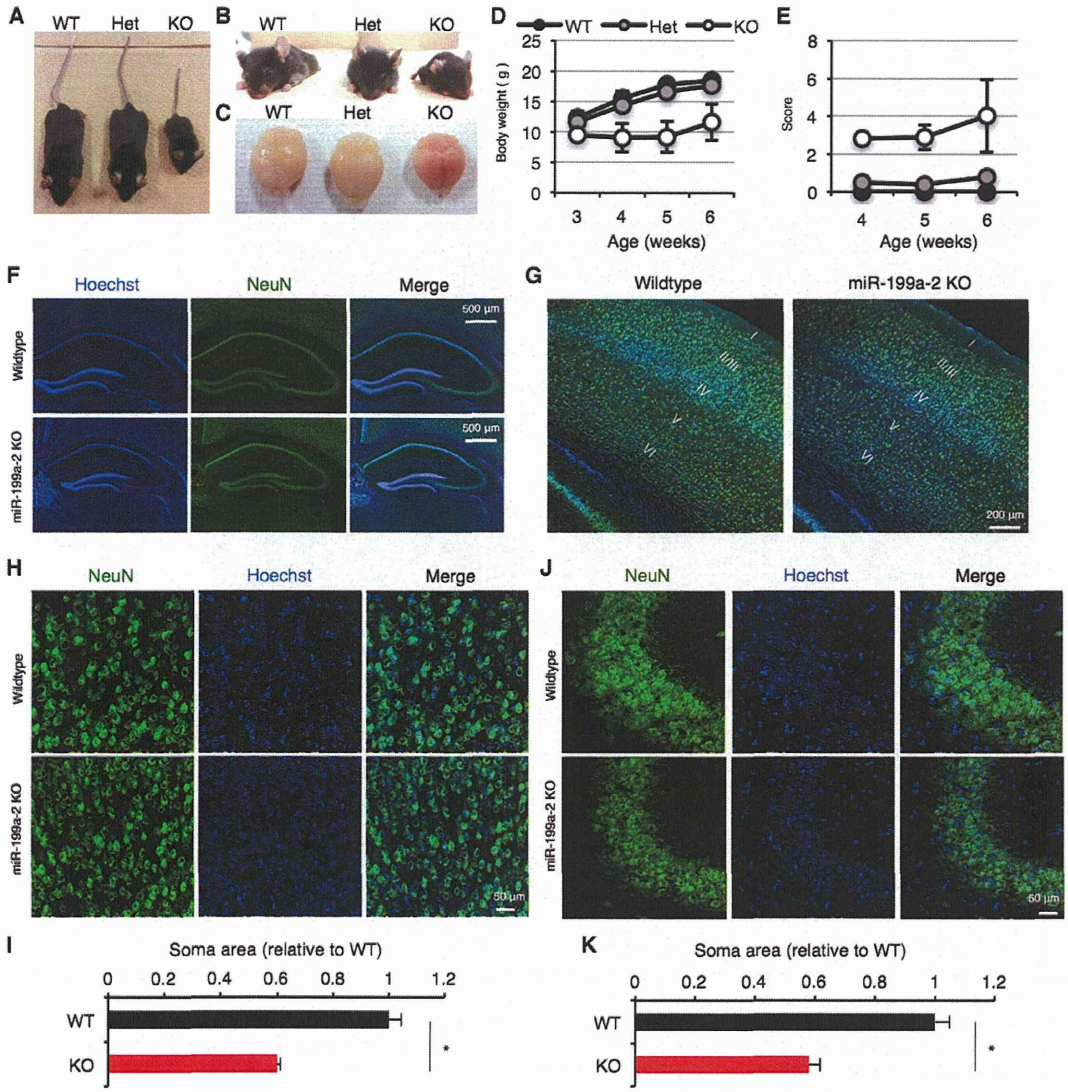

Figure 6. Loss of miR-199a-2 Recapitulates RTT Phenotypes

(A and B) Comparison of body size of WT, heterozygous (Het), and miR-199a-2 KO littermates.

(C) Comparison of brain size of WT, Het, and miR-199a-2 KO littermates.

(D) miR-199a-2 KO mice body weight is less than that of WT and Het littermates (measured from postnatal 3–6 weeks). Data are represented as mean ± SEM. n = 3–5.

(E) Plots of the phenotypic scores of WT, Het, and miR-199a-2 KO littermates. Data are represented as mean ± SEM. n = 3–6.

(F) Representative immunohistological images of WT, Het, and miR-199a-2 KO hippocampi. Brain sections at 6 weeks were stained with anti-NeuN (green) antibody and Hoechst 33258 (blue). Hippocampus size of miR-199a-2 KO is smaller than that of WT, but abnormal structural changes were not observed.

(G) Representative immunohistological images of WT and miR-199a-2 KO cortices. Brain sections at 6 weeks were stained with anti-NeuN (green) antibody and Hoechst 33258 (blue). Abnormal structural changes are not detected in miR-199a-2 KO brain.

(H) Representative immunohistological images of cortical layer II/III regions of WT and miR-199a-2 KO mice. Brain sections at 6 weeks were stained with anti-NeuN (green) and Hoechst 33258 (blue). Decreased soma size of neurons and increased neuronal packing density were observed in miR-199a-2 KO mice.

(I) Quantification of neuronal soma size in (H). *$p < 0.05$ compared to WT; n = 9 sections (n = 3 brains of each genotype).

(J) Representative immunohistological images of hippocampus CA3 regions of WT and miR-199a-2 KO mice. Brain sections at 6 weeks were stained with anti-NeuN (green) and Hoechst 33258 (blue). Decreased soma size of neurons and increased neuronal packing density are observed in miR-199a-2 KO mice.

(K) Quantification of neuronal soma size in (J). *$p < 0.05$ compared to WT; n = 9 sections (n = 3 brains from each genotype).

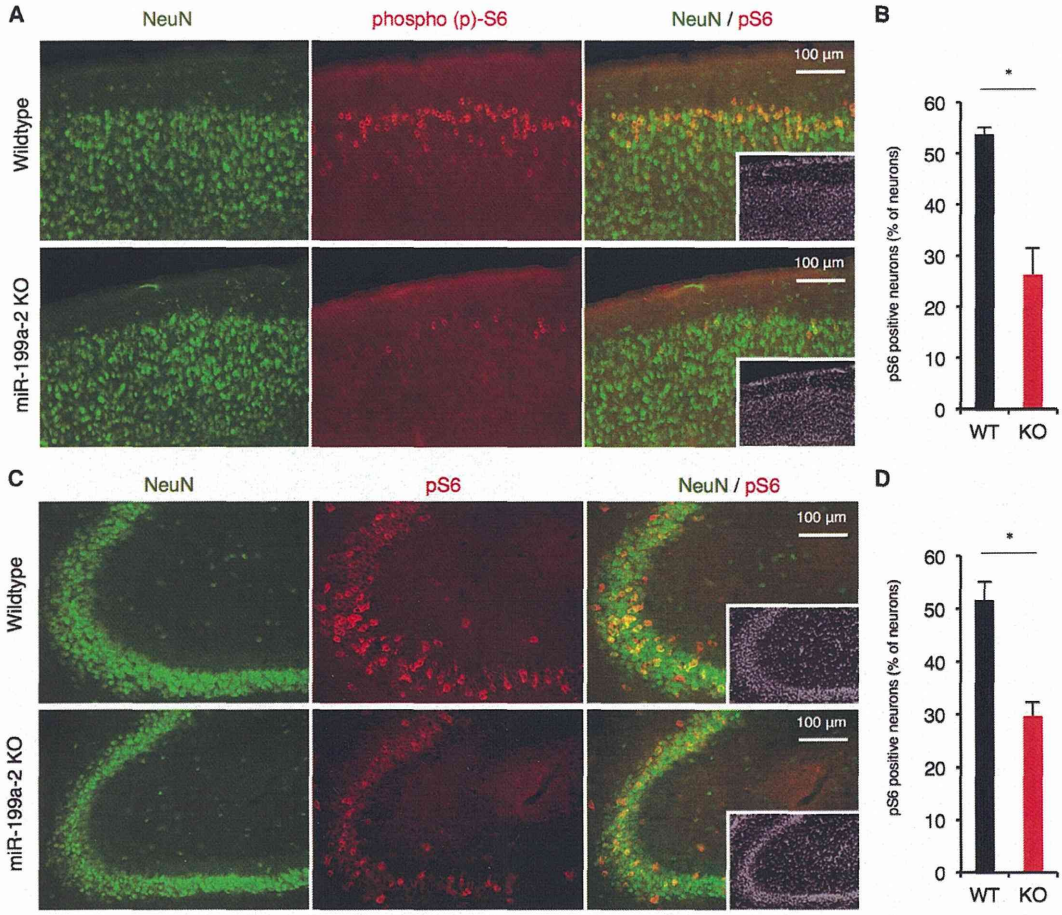

Figure 7. Loss of miR-199a-2 Results in a Decreased mTOR Activity in the Brain

(A) Representative immunohistological images of WT and miR-199a-2 KO cortices. Brain sections at 6 weeks were stained with anti-NeuN (green) and p-S6 (red) antibodies. mTOR activity in the cortex was markedly reduced in miR-199a-2 KO mice.

(B) pS6-positive neurons in (A) were quantified. *$p < 0.05$ compared to WT; n = 9 sections (n = 3 brains from each genotype).

(C) Representative immunohistological images of hippocampus CA3 regions of WT and miR-199a-2 KO mice. Brain sections at 6 weeks were stained with anti-NeuN (green) and p-S6 (red) antibodies. mTOR activity in the hippocampus dramatically reduced in miR-199a-2 KO mice.

(D) pS6-positive neurons in (C) were quantified. *$p < 0.05$ compared to WT; n = 9 sections (n = 3 brains from each genotype). Nuclei are visualized by Hoechst staining (A and C, insets).

pmirGLO-*Pde4d*, *Sirt1*, *Hif1α-3′* UTR-Mut using Lipofectamine 2000. After transfection, the cells were incubated for 6 days and lysed with reporter lysis buffer. Luciferase activity of the lysates was measured with the Dual-Glo Luciferase Assay System (Promega) according to the manufacturer's protocol. Firefly luciferase activities were determined by three independent transfections and normalized by comparison with the Renilla luciferase activities of the internal control.

Scoring of Symptoms

Neurological symptoms of mice were scored as previously described (Guy et al., 2007).

Statistical Analysis

The results presented are the average of at least three experiments, each performed in triplicate, with SEs. Statistical analyses were performed by one-way ANOVA, followed by Tukey's or Bonferroni multiple comparison tests, or by Student's t test as appropriate, using Prism 5 (GraphPad Software). Probabilities of $p < 0.05$ were considered significant.

ACCESSION NUMBERS

The DNA DATA Bank of Japan (DDBJ) Sequence Read Archive (DRA) databank accession number for all deep sequencing data reported in this paper is DRA: DRA002731, which includes data sets of neurons and NSCs.

SUPPLEMENTAL INFORMATION

Supplemental Information includes Supplemental Experimental Procedures, six figures, and two tables and can be found with this article online at http://dx.doi.org/10.1016/j.celrep.2015.08.028.

AUTHOR CONTRIBUTIONS

K.T. conceived the original ideas, designed the project, and wrote the paper. K.T. performed the majority of the experiments with participation from K.I. and H.N. Y.N. contributed to experiments about SIRT1. S.T. and Y.E.